Polymer 49 (2008) 4713–4722

Contents lists available at ScienceDirect

Polymer

journal homepage: www.elsevier.com/locate/polymer

Effect of fiber diameter on tensile properties of electrospun poly(ε-caprolactone)

Shing-Chung Wong [a,*], Avinash Baji [a], Siwei Leng [b]

[a] Department of Mechanical Engineering, The University of Akron, Akron, OH 44325-3903, USA
[b] Institute of Polymer Science, The University of Akron, Akron, OH 44325-3903, USA

ARTICLE INFO

Article history:
Received 30 July 2008
Accepted 9 August 2008
Available online 16 August 2008

Keywords:
Electrospinning
Nanofibers
Tensile properties

ABSTRACT

The tensile properties of electrospun fibers have not been widely investigated due to the difficulties in handling nanofibers and measuring low load for deformation. In this study, the effect of dimensional confinement on free standing biodegradable poly(ε-caprolactone) (PCL) is investigated using electrospinning-enabled techniques and a nanoforce tensile tester. The structural properties such as crystallinity and molecular orientation of the spun fibers are examined using wide angle X-ray diffraction (WAXD). The degree of crystallinity and molecular orientation of fibers are enhanced when the diameter of spun fibers is reduced, resulting in improved mechanical strength and stiffness. It is evident that PCL fibers with decreasing fiber diameter exhibit an abrupt shift in tensile performance in comparison to those derived from non-spun systems. The abrupt shift in tensile strength and stiffness of electrospun PCL fibers occurs at around 700 nm in diameter and illustrates the importance of studying the mechanical behavior of the nanofibers, for the first time, systematically with the aid from electrospinning techniques. This shift cannot be otherwise explained by a noticeable change in T_g, and the gradual increase in crystallinity and molecular orientation.

1. Introduction

Recent advances in nanostructured biomaterials have led us to revisit the bio-inspired phenomena that are essential to understand the superior performance of heterogeneous materials that occur at the nanometer length scale. Nanostructured biomaterials possess superior mechanical strength despite the comparatively poor performance of their constituents when tested alone [1–3]. Natural biomaterials are self-assembled in an orderly pattern of organic matrix and mineralized organics in the sub-micrometer and nanometer length scales providing superior strength and fracture resistance [4]. Such material systems include the widely studied nacre, enamel and bone. The structure of polymeric constituents is geometrically confined in the nanometer and micrometer length scales and helps these natural materials to attain the theoretical values for intramolecular and intermolecular boundary separations [1–9] and, hence, optimizes the mechanical properties of the resulting composites. Despite the widely held belief that the confinement effects of nacre and enamel are derived from the reinforcing minerals or mineral platelets on polymers, there is very little understanding pointing to the possibility that the polymers are spatially confined by the characteristic length such that the fiber diameter approaches that of the radius of gyration of the molecular chains. This lack of understanding is further exacerbated by the fact that simple mechanical properties such as stiffness and strength of plastics are seldom measured with accuracy and reliability when they are made into structures the size of the polymer molecules themselves, which are just tens of nanometers in diameter. Our studies [10,11] indicate that the macromolecules need to form uniquely different geometric orientations in order for them to appear in dimensions from 10 nm (near the radius of gyration) to 1000 nm like the bulk specimens. This concept is analogical to the well-established plane stress to plane strain transition in measuring the specific essential work of fracture in polymer films [12,13]. As the specimen ligament approaches zero in length, the material is severely constrained and cannot exhibit profuse plastic deformation, resulting in plane strain, instead of plane stress, fracture toughness assessment. As the polymer molecules are spatially limited in nano-confined state, the nanoscale fibers ought to re-arrange themselves to accommodate dimensional constraints for enhanced mechanical behavior.

In this study, confinement refers only to limiting spatial arrangement of PCL molecules in cylindrical shapes with diameter ranging from two hundred to several hundred nanometers, such as in electrospun nanofibers. Such spatial confinement produces flaw insensitive [6] nanofibers that are compression molded into bulk geometry as compared to a compression molded specimen from pellets. The confinement resulting from the processing condition

* Corresponding author. Tel.: +1 330 972 8275; fax: +1 330 972 6027.
E-mail address: swong@uakron.edu (S.-C. Wong).

0032-3861/$ – see front matter © 2008 Elsevier Ltd. All rights reserved.
doi:10.1016/j.polymer.2008.08.022

can affect the material's structure, macromolecular conformation and mechanical characteristics resulting in superior properties [14]. Recently, Arinstein et al. [7] reported an abrupt increase in Young's modulus when the supramolecular structural dimension is comparable to the nanofiber diameter. Their findings challenge the commonly held view that surface/boundary effects are most significant for deformation in nanofibers. Modeling the strength and toughness of nacre, Katti and Katti [8] demonstrated that nanoscale asperities play only a marginal role in the strengthening and toughening of the natural composite. Their results reinforce the notion that confined proteinaceous molecules in between the aragonite platelets play a more substantial role in the synergistic toughness and strength of nacre, which by nature is a polymer–mineral composite. Hence, the mechanical response of a polymeric system within a certain degree of spatial confinement needs to be investigated in detail in order for materials designers to mimic the nanostructure of biomaterials for superior mechanical properties.

In this paper, we utilize the versatile electrospinning technique to produce polymer nanofibers such that we can, for the first time, systematically evaluate the phenomena arising from spatially limited polymers. We test the hypothesis that the mechanical properties of electrospun polymer nanofibers are influenced by the fiber diameter, molecular geometry, molecular orientation and degree of crystallinity. In this study we employ X-ray diffraction techniques to evaluate the effect of electrospinning process on the structures of spun polymer fibers. The change in crystallinity and molecular orientation as functions of fiber diameters and tensile strains is reported. This study demonstrates that the nanometer-scale (250–1000 nm) fibers produced by electrospinning can effectively result in strikingly superior tensile strength and modulus with the same specimen dimensions of the bulk and loading rates.

2. Experimental work

2.1. Materials

The biodegradable polymer, polycaprolactone (PCL) ($M_w = 80{,}000$ g/mol) is obtained from Dow Chemical Company (Freeport, TX) and 2% Mg doped hydroxyapatite nanopowder (HAP) of particle size 50–100 nm is purchased from nGimat™ (Atlanta, GA). PCL pellets are dried under vacuum at 40 °C for 24 h and are used to produce spun and non-spun specimens.

2.2. Bulk (non-spun) specimen processing

For comparative studies, non-spun samples of PCL are prepared by one-step compression molding. The PCL pellets are compression molded at 130 °C and 275 bar in pressure. The thickness of the specimens is controlled by using compression molding plates of 0.5 mm in thickness. The specimens for mechanical tests are then cut from the molded sheet to obtain dog bone shaped specimens ($3.15 \times 63.15 \times 0.5$ mm^3). This batch of specimens is labeled as Sample 1 in Table 1.

A separate batch of non-spun samples is prepared to study the mechanical behavior of hydroxyapatite (HAP) reinforced PCL composites. PCL pellets with varying HAP concentration (0–30 wt%) are extruded using Haake mini-lab twin screw extruder (Thermo Electron Corp., Hamburg Germany) at 130 °C. The screw speed was 80 rpm and the residence time was 6 min. The extruded material was injection molded into dog bone specimens ($3.17 \times 63.5 \times 3.17$ mm^3) for mechanical testing.

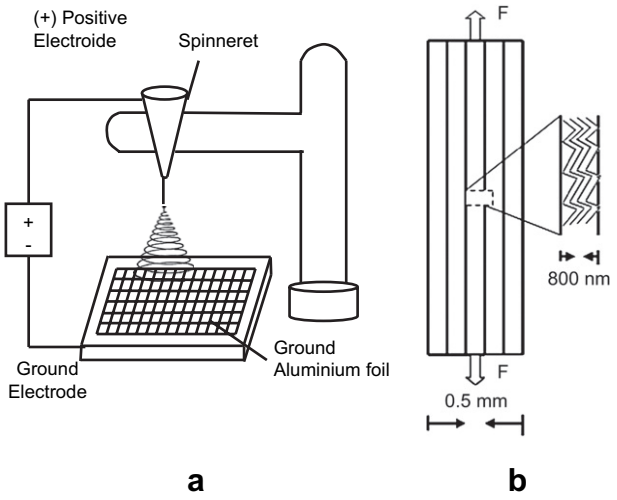

Fig. 1. Schematics of (a) an electrospinning setup and (b) the compression molded electrospun PCL fiber sheets. The spatially confined PCL molecules from compression molding the electrospun fibers are illustrated.

2.3. Electrospinning

Electrospinning technique is used to prepare ultrafine polymer nanofibers for mechanical and WAXD studies. This process uses high electrical forces to electrically charge a polymer solution. The electrical force overcomes the surface tension of the solution and ejects out a jet of solution, which solidifies into ultrafine polymer fibers. The electrical force accelerates and stretches the polymer jet resulting in a decrease of the diameter and concomitant increase in the length. The jet dries, solidifies and is collected on a conductive ground collector [15,16]. The electrospinning setup used is shown in Fig. 1a. Fig. 1b illustrates that the spun fibers [15,16] also simultaneously extend and align the molecules in the axial direction.

The polymer solution for electrospinning is prepared by dissolving known percentage of polymer pellets in two types of solvents (acetone and dimethylformamide/chloroform mixture). The concentration of PCL in the solution and the solvent is chosen to control the diameters of the fibers from 250 nm to 2.5 μm for single fiber testing, and, independently from 250 to 900 nm for wide angle X-ray diffraction studies. The finer fiber diameter is obtained by increasing the concentration of dimethylformamide (DMF) in the solvent mixture. The presence of DMF increases the splaying and splitting, resulting in thinning of the jet. The polymer solution is mechanically stirred for 3–4 h and stored under vacuum prior to use.

The solution of PCL is electrospun without any further processing as described above. The fibers are deposited on a grounded flat metal plate and are collected as electrospun layer sheet. Layers of spun PCL sheets with randomly oriented fibers are collected and compression molded at 50 °C. Specimens with dimensions $3.17 \times 63.17 \times 0.5$ mm^3 are then cut from the compression molded

Table 1
Comparison of spun and non-spun compression molded samples.

Sample number	Processing method	Specimen dimension (mm^3)	Elastic modulus (MPa)	Tensile strength (MPa)
1	Compression molded	$3.15 \times 63.15 \times 0.5$	237 (5.85)	14 (0.98)
2	Compression molded electrospun sheet	$3.17 \times 63.17 \times 0.5$	307 (6.02)	58 (3.63)

An average of five specimens was tested for each sample (standard deviations in parentheses).

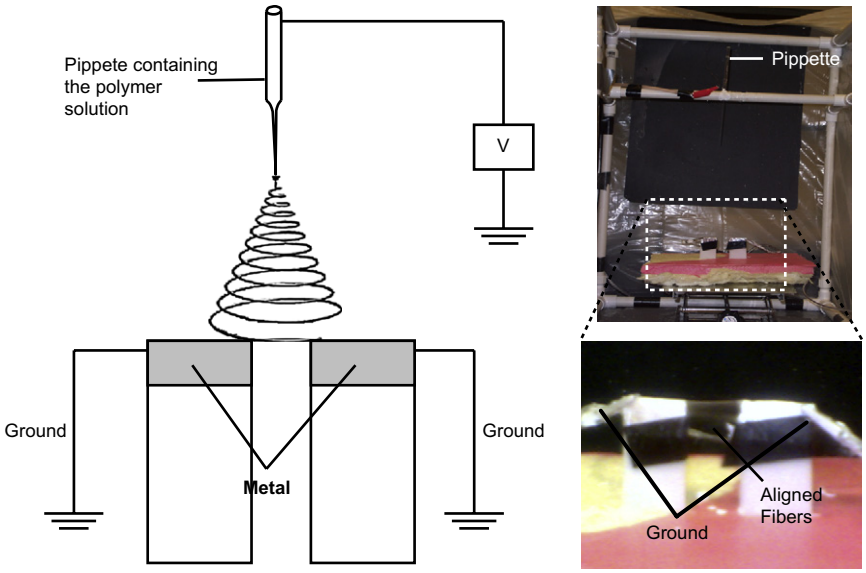

Fig. 2. Schematic of the method used to collect single and aligned fibers. These aligned fibers are collected as bundles and used for WAXD tests. The single fibers are collected on the cardboard sheet using double sided adhesive tape for mechanical testing.

electrospun sheets. These specimens are labeled as Sample 2 in Table 1. It is assumed that Sample 2 shares comparable density as Sample 1 following the compression molding process. The fibers in the molded-spun samples are measured to have 800 nm in diameter on average. The effect of spatial confinement of nanofibers on mechanical properties is evaluated by comparing the mechanical behavior of Sample 1 and Sample 2.

A separate process of electrospinning is used to evaluate the mechanical behavior of PCL fibers with HAP inclusion. This batch of samples is prepared by dispersing known concentration of HAP (0–30 wt%) in the PCL solution prior to electrospinning process. The solution is then stirred for 1–2 h. Using the electrospinning setup as described above, the solution is electrospun. Tensile specimens ($3.10 \times 55.12 \times 0.008\ mm^3$) are then trimmed from the collected spun sheet. The thickness of each tensile specimen is determined using stereomicroscopes (Leica S6D and Leica DMLB2).

2.4. Aligned electrospun fibers

To analyze the effect of fiber diameter on the mechanical properties, two non-conductive strips of materials are placed along a straight line and an aluminum foil is placed on each of the strips and connected to the ground as shown in Fig. 2. This technique enables fibers to be deposited at the end of the strips such that the fibers adhere to the strips alternatively and collected as aligned array of fibers. This fiber collection is for short duration (~5 s) for a few aligned single fibers. The fibers will then be mounted on a trimmed cardboard sheet with double sided tape as shown in Fig. 3. They will be trimmed under the microscope to leave exactly one fiber intact on the cardboard sheet enabling the testing of individual fibers.

2.5. Mechanical testing

Non-spun samples (Sample 1 and samples processed using extrusion followed by compression molding) and molded-spun sample (Sample 2) are tested using an Instron 5582 at 10 mm/min. An ultra-sensitive testing equipment is used to measure the load vs. strain for spun samples and single fibers. The specimens are tested using an MTS NanoBionix® (MTS Systems Corporation, Oak Ridge, TN, USA) with a load resolution of 50 nN and extension resolution of 35 nm. The loading rate reading from the specialized NanoBionix is 10%/s. The procedures to quantify the number of fibers and fiber diameters for spun samples are done in a similar fashion as reported by Pham et al. [17]. The volume of fiber phase is determined carefully from representative micrographs to calculate the stress on the fibers. SEM images are taken across the width of the specimen and average fiber area density is quantified by counting the number of fibers that intersects the line drawn across the SEM image. Stress is then obtained to be the ratio of the load measured to the total fiber area revealed by micrographs.

2.6. Wide angle X-ray diffraction (WAXD)

Wide angle X-ray diffraction is performed on the samples to determine the degree of crystallinity and molecular orientation within the material. WAXD analysis is performed on bundles of aligned fibers as described in Section 2.4. The electrospinning process is run for a longer duration of time (~2 min) such that bundles of aligned fibers can be collected.

The one-dimensional (1D) WAXD experiments are carried out using Ni filtered Cu K_α radiation from a Rigaku 2 kW X-ray tube generator with divergence, receiving, and scattering slits. The two-dimensional (2D) WAXD experiments are studied through a Rigaku 18 kW rotating anode X-ray generator attached with R-AXIS-IV image plate system. Crystallinity and molecular orientation on bundles of aligned fibers are determined when strained to 0, 10, 20

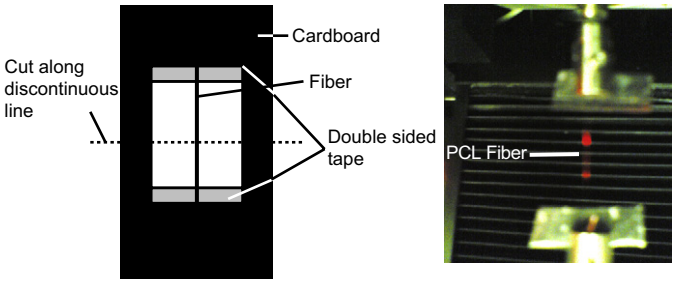

Fig. 3. Method used for testing single fibers. The diameter of the fibers is determined prior to testing. The single fibers along with the cardboard sheet are fixed between the grips of the NanoBionix. The cardboard sheet is cut along the discontinuous line as shown so that the load is experienced by the fibers.

and 40%. The fibers are stretched prior to the X-ray analyses and the strain level (%) is maintained. The degree of crystallinity for the samples is determined using PEAKFIT software on the WAXD pattern. The area under the peaks divided by the total area under the curve is used to estimate the crystallinity.

2.7. Calculation of draw ratio and elongation rate

The draw ratio for the PCL fibers is calculated to support the claim that electrospinning elongates and stretches the fibers under the influence of electric field. During the electrospinning process, the PCL solution experiences shear flow. The solution is then ejected from the pipette followed by the elongation of the jet under the influence of electrostatic force. The fluid instability in the jet causes whip-like motion in the jet, thereby increasing the degree of stretching before reaching the ground collector. The amount of elongation the PCL material experiences can be measured and can be quantified using the draw ratio.

The draw ratio for spun PCL fibers is calculated to be the ratio of spinning velocity of the collected fiber to ejection velocity of the PCL solution from the pipette [18–21]. The velocity of the fibers at the ground collector is calculated as:

$$v_{\text{spin}} = w_{\text{f}}/100\rho_{\text{f}}\pi\left(r_{\text{f}}\right)^2 t \quad (1)$$

where v_{spin} is the spinning velocity (m/min) when the fibers are collected at the ground electrode. w_{f} is the weight (g) of the PCL fibers on the ground electrode, ρ_{f} is the density (g/cc) of the PCL fibers, r_{f} is the average radius (cm) of the collected fibers and t is the electrospinning time (min). The electrospinning process was run for ~50 min.

The ejection velocity of the PCL solution from the pipette is given by the equation:

$$v_{\text{sol}} = w_{\text{sol}}/100\rho_{\text{sol}}\pi(r_{\text{p}})^2 t \quad (2)$$

where v_{sol} is the ejecting velocity (m/min) of the PCL solution, w_{sol} the weight (g) of the PCL solution at a certain time during electrospinning, ρ_{sol} the density (g/cc) of the PCL solution, r_{p} the diameter (cm) of the pipette used and t the electrospinning time (min). Using Eqs. (1) and (2), the draw ratio is determined to be the ratio of $v_{\text{spin}}/v_{\text{sol}}$ [18–21]. The diameter of the fibers and the pipette was measured using optical microscope.

The elongation rate of the PCL fibers during the electrospinning process is determined using the equation

$$\varepsilon = (v_{\text{spin}} - v_{\text{sol}})/l \quad (3)$$

where ε is the elongation rate and l is the distance between the pipette and ground collector.

2.8. Scanning electron microscopy (SEM)

Samples for SEM analysis are mounted on the aluminum stub using carbon coated double sided adhesive tapes. The surface is coated with silver using a sputter coater in an argon-purged chamber evacuated to 500 mTorr with an accelerating voltage of 20 kV.

2.9. Thermal analyses

The melting points (T_{m}) and the glass transition temperature, T_{g}, for Samples 1 and 2 is determined using the dynamic scanning calorimetry (DSC) and dynamic mechanical analyzer (DMA), respectively. DSC analysis is performed on TA instruments DSC at 5 °C/min. DMA analysis is performed using a Perkin–Elmer DMA7 model.

3. Results and discussions

3.1. Effect of electrospinning on mechanical properties of spun and non-spun samples

The tensile properties of the tested specimens (Samples 1 and 2) are summarized in Table 1. An average of five specimens was tested for each sample type. The representative stress–strain curves of Samples 1 and 2 are shown in Fig. 4. The modulus and tensile strength of Sample 2 are superior to Sample 1 prepared with conventional one-step compression molding of pellets. Their stress–strain curves are drastically different. Sample 2 exhibits an average tensile strength (>58 MPa) more than three-fold that of Samples 1 obtained from non-spun systems (~14 MPa). Samples 1 and 2 illustrate the contrasting phenomena enabled by electrospinning. Interestingly, they yield drastically different tensile performance despite sharing the same specimen size, dimensions, and also loading rate (10 mm/min). Noteworthy in Fig. 4 is electrospinning completely eradicates the necking displayed by the non-spun samples on their stress–strain curve. By comparing the two specimens of equal dimensions, we eliminate the variation in parameters that can be derived from mechanics considerations, with the resulting change that can only be attributed to the nanofiber-structured phenomenon introduced *a priori* by electrospinning. Sample 1 exhibits lower tensile strength and modulus than Sample 2 but Sample 1 has a higher elongation at break. Fig. 5 shows the SEM morphology of the molded-spun specimens. The SEM image shows that the fiber texture is clearly visible after compression molding.

3.2. Thermal properties of spun and non-spun samples

The specific melting enthalpies of the samples were determined from the DSC thermograms. The peak of the tan δ vs. temperature curves represents T_{g} values for the specimens studied. The melting point, T_{m}, and the T_{g} values for Samples 1 and 2 are determined to be 60 °C and −60 °C, respectively, as shown in Figs. 6 and 7. There is no observable change due to the electrospinning process in the T_{m} and the T_{g} values, which are indicative of the characteristic crystal and amorphous domains in the semi-crystalline PCL. Note that the spun fibers in this thermal analysis are on average 800 nm in diameter. T_{g} values for electrospun samples, as expected, are not found to decrease since the diameter of the fibers in Sample 2 is

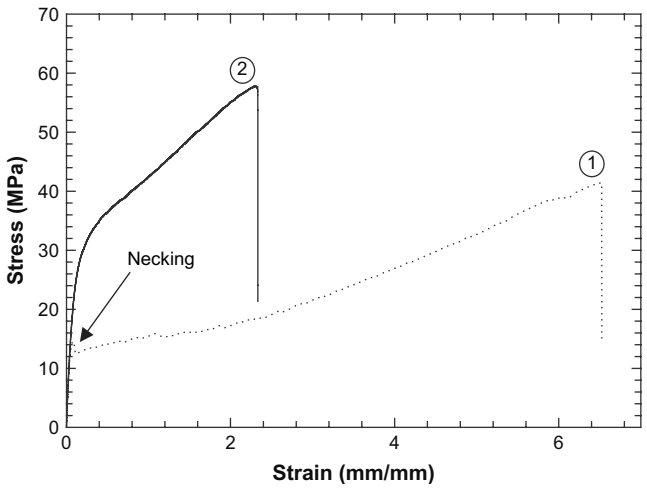

Fig. 4. Representative stress–strain curves of Samples 1 and 2. Sample 2 (curve 2) exhibits significantly higher tensile strength and modulus compared to Sample 1 (curve 1).

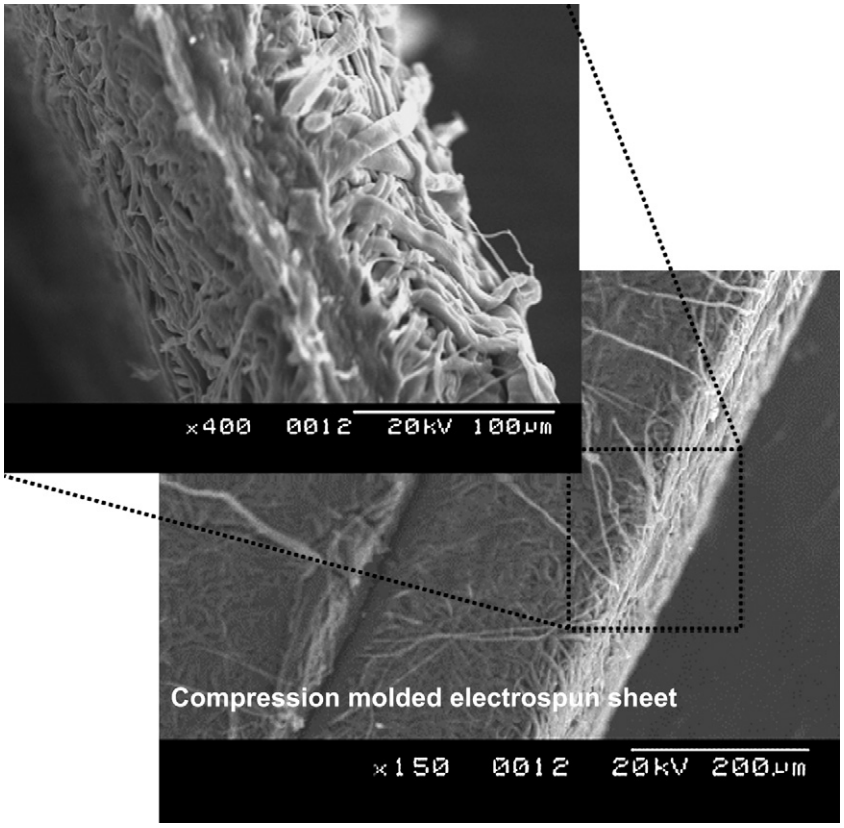

Fig. 5. SEM micrograph of the compression molded electrospun PCL fiber sheet. The electrospun fibrous structures (~800 nm in diameter) are preserved after compression molding at 50 °C.

much larger than the radius of gyration (~2.25 nm) for PCL molecule. It is evident that Samples 1 and 2 exhibit similar melting peaks and show no change in the specific melting enthalpies. The consistent thermal properties also confirm that the mechanical properties presented in Section 3.1 derived from the two processing routes for Samples 1 and 2 can be meaningfully compared. Ngai [22,23] argued that the decrease in T_g is usually seen when one of the dimensions is reduced below a critical value, which is the end-to-end distance of the polymer molecule. For dimensions above this critical length scale, the T_g values do not show a significant difference due to the presence of intermolecular coupling between polymer chains. Intermolecular coupling decreases as the fiber diameter decreases and approaches a critical length scale. In the case of 800 nm, it appears that the fiber diameter is above the length scale for which T_g decreases.

3.3. Tensile properties of ultrafine single fibers of PCL

Tensile tests were performed on single fibers of unreinforced PCL with diameters ranging from 350 nm to 2.5 µm. Fig. 8 shows some representative stress–strain curves obtained from single fiber testing using the nanoforce tensile tester. All other fibers tested demonstrate similar trends in the stress–strain curves. The

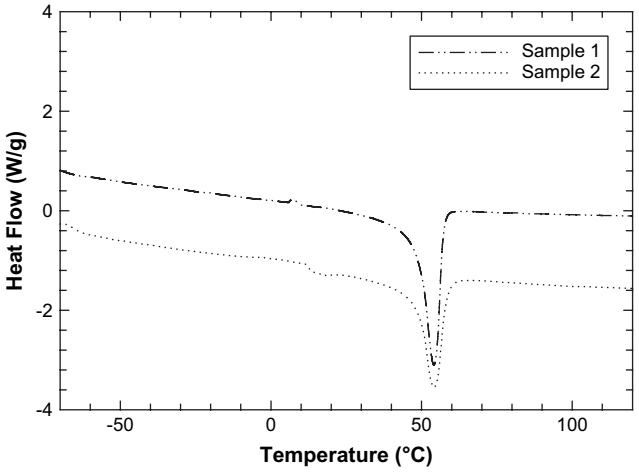

Fig. 6. DSC curves of Samples 1 and 2 comparing the melting temperature and heat of fusion.

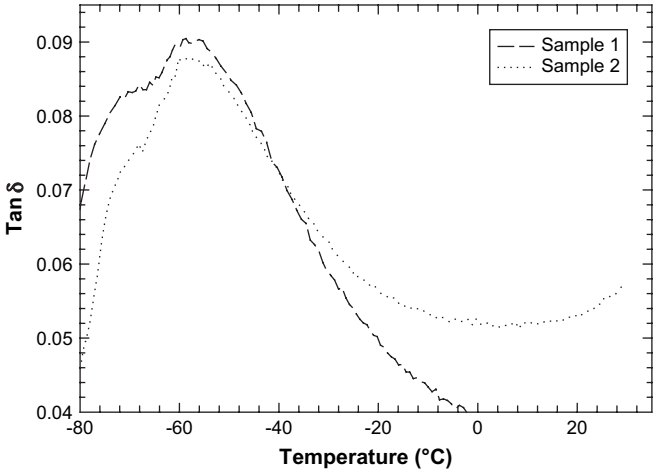

Fig. 7. DMA curves of Sample 1 and 2. The T_g of the samples was recorded at the peaks of the tan(δ) curves.

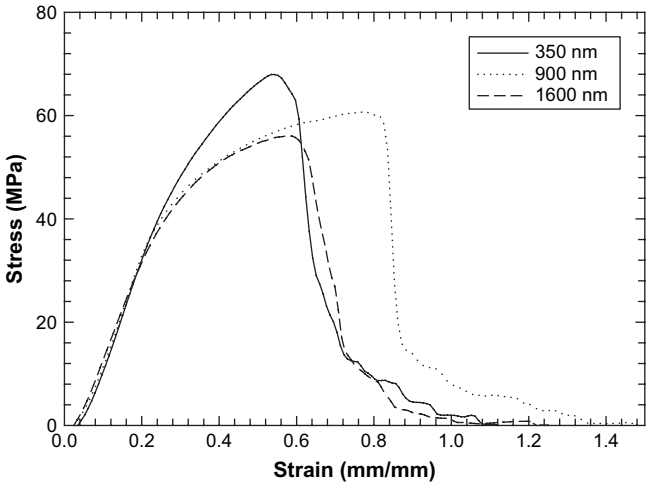

Fig. 8. Representative stress–strain curves of single fibers obtained from tensile tests. Fibers with small diameters are seen to have higher modulus and strength.

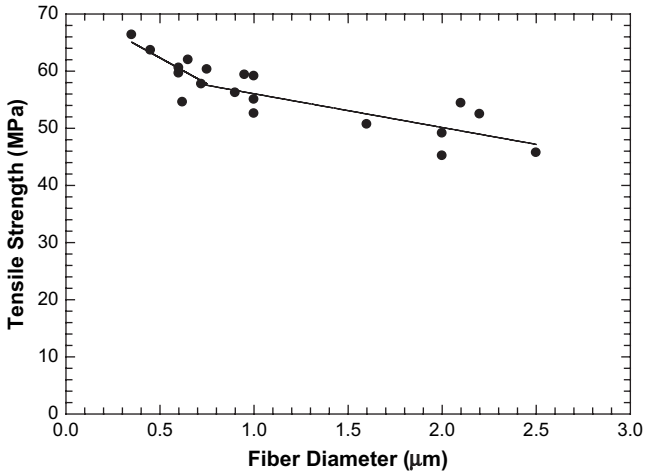

Fig. 10. Plot of tensile strength vs. fiber diameter. Tensile strength increases with a decrease in fiber diameter. This result can be attributed to better molecular orientation among smaller fiber diameters as seen from WAXD results.

deformation mechanism of all the fibers tested is consistent with the mechanisms noted from spun composite samples. These electrospun fibers do not exhibit the necking phenomenon. Figs. 9 and 10 show the tensile modulus and tensile strength vs. fiber diameter, respectively. The modulus and strength of the fibers increase as the fiber diameter decreases. However, an abrupt change in tensile modulus and strength can be clearly seen in the proximity of ~700 nm in diameter. Note that the data shown in Figs. 9 and 10 are derived from the stress–strain curves produced by the sensitive nanoforce tensile tester as described in Section 2.5. Similar shifts in the tensile properties in the intermediate (~500 nm) regime had been reported by other investigators [7,24,25] but their observations were not examined systematically in light of X-ray diffraction data. The effect of fiber diameter on tensile stiffness and strength becomes more predominant for fibers with diameters less than ~700 nm. The ductility of the fibers decreases as fiber diameter decreases. The abrupt increases in modulus and tensile strength values of electrospun PCL fibers due to the size effect are also discussed independently by Arinstein et al. [7], Lim et al. [24] and Chew et al. [25].

The molecules in semi-crystalline polymers form a soft and a hard phase. The soft phase is known as the amorphous phase which provides the elastomeric characteristics whereas the hard phase forms the crystalline phase and imparts dimensional stability to the array of molecules. The random or ordered arrangement of the amorphous and crystalline phases determines the physical and the mechanical properties of the semi-crystalline polymers. The deformation mechanisms in the intermediate scale fibers are entirely different from the deformation mechanism observed in bulk or microscopic fibers. Arinstein et al [7] argued that the orientation of the macromolecules is present in the supramolecular structures of the amorphous phase and plays a dominant role in the abrupt increase of mechanical properties of fibers when the diameter is comparable to the critical threshold scale. The enhanced mechanical behavior of the fibers was attributed to the dimensional effects and mode of deformation of the fibers. In Section 3.4, the crystallinity effect will also be investigated.

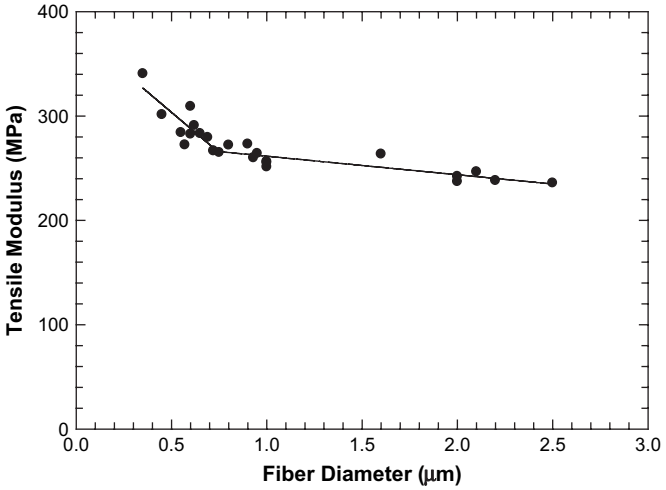

Fig. 9. Plot of tensile modulus vs. fiber diameter. Tensile modulus increases with a decrease in fiber diameter. This result can be attributed to better molecular orientation and crystallinity among smaller fiber diameters as seen from WAXD results.

Lim et al. [24] demonstrated that the finer fibers are obtained when the polymer jet stretches to a greater extent during the electrospinning process, resulting in higher orientation of macromolecular chains. The drawing effect is increased for finer diameter fibers collected and is responsible for the enhanced tensile behavior of finer fibers. They suggested that the densely packed lamellae and fibrillar structures align themselves and play an important role in enhancing the mechanical properties for finer diameter PCL fibers. The fibrillar structure has a high degree of molecular orientation and provides high resistance to axial tensile force. As the diameter of fiber increases, the lamellae tend to re-orientate and the presence of alignment and fibrillar lamellae structure decreases, resulting in reduced mechanical properties.

In our study, we evaluate the enhanced properties due to the reduction in fiber diameter using the draw ratio. During the electrospinning process, the polymer jet travels a long distance before reaching the ground electrode. The use of electric field during the process spontaneously aligns the highly mobile molecular chains in the direction of fiber axis, resulting in the higher degree of molecular orientation. The fibers produced are extremely rapid and experience huge material elongation rate and reduction in the cross-sectional area (order of 10), which affect the orientation of structural elements within the fibers. As a result the polymer jet undergoes large draw ratios. These structural characteristics, including crystallinity and molecular orientation, influence the mechanical properties of the electrospun fibers. The observed physical properties of the fiber are analyzed by determining the relationship between the draw ratio and fiber diameter. Fig. 11 shows the relationship between fiber diameter and draw ratio. The

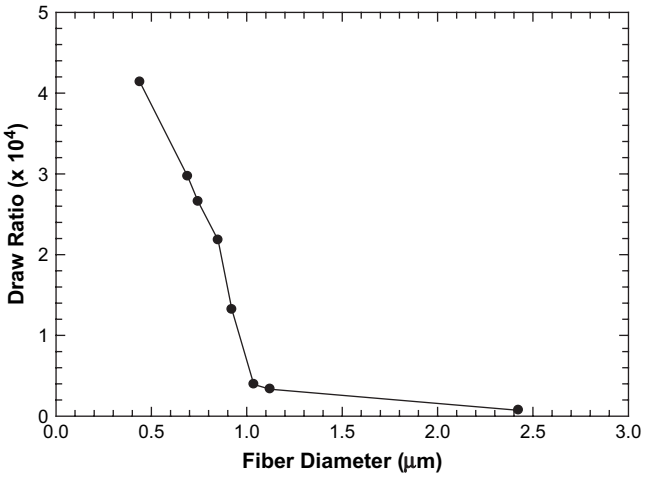

Fig. 11. Plot of draw ratio vs. fiber diameter. The draw ratio for the PCL fibers increases as the fiber diameter is decreased.

draw ratio values calculated using Eqs. (1) and (2) as discussed in Section 2.7 represent the degree of melt stretching in the polymer fibers during the electrospinning process. Comparable trends are observed in the draw ratio vs. fiber diameter as the tensile properties vs. fiber diameter. However, the two parameters cannot be equated with each other. This is because the abrupt shifts appear at slightly different fiber diameters: 700 nm for tensile properties and 900 nm for draw ratio. Draw ratio generally increases with the decrease in fiber diameter. This is consistent with the trends in tensile properties as shown in Figs. 9 and 10. The draw ratio value at ~900 nm fiber diameter abruptly increases rapidly and reaches 10^4 in orders of magnitude. The spinning velocity increases to 26 cm/s and the elongation rate increases by an order of $\sim 10^2$ for 600 nm fiber diameter. This suggests an abrupt alteration in the alignment of the amorphous molecules and possibly the polymer crystals when the fiber diameter approaches below 900 nm. Similar observations on an abrupt shift in tensile properties were reported by other investigators [7,24] despite the abrupt shift in tensile properties was not emphasized. Therefore, it can be concluded that PCL macromolecular chains are extended by a step-wise increase in draw ratio. And, it would be expected that the PCL fibers exhibit also a step-wise increase in tensile properties. The fibers experience a transition from microscale to nanoscale deformation as the size of the fiber is reduced from 1000 to 600 nm. Despite this range of fiber diameters is considerably higher than the expected radius of gyration, R_g, of PCL (~2.25 nm) [26], evidence exists [7,27] that the transitional behavior in terms of the crystalline morphology takes place well above the R_g values and polymer relaxation behavior drastically changes as a function of polymer film thickness [22,23,27]. The examination of the transitional mechanisms is beyond the scope of our present study. Nonetheless, the fiber diameter at which such a transition takes place should be a characteristic of the polymer (PCL in this paper).

3.4. WAXD study on aligned fibers as a function of fiber diameter

X-ray analysis was performed on aligned fiber bundles to verify the relationship between crystallinity and molecular orientation with respect to the diameter of the fibers. Before this there was little work performed on understanding the relationship between fiber diameter and the molecular orientation and crystallinity in the intermediate nanoscale domain. X-ray analyses are performed on aligned fibers with various fiber diameters, viz., 250, 400, 600, 800 and 900 nm. Fig. 12 shows the WAXD pattern of aligned fibers performed on two sets of fibers diameter (250 and 900 nm)

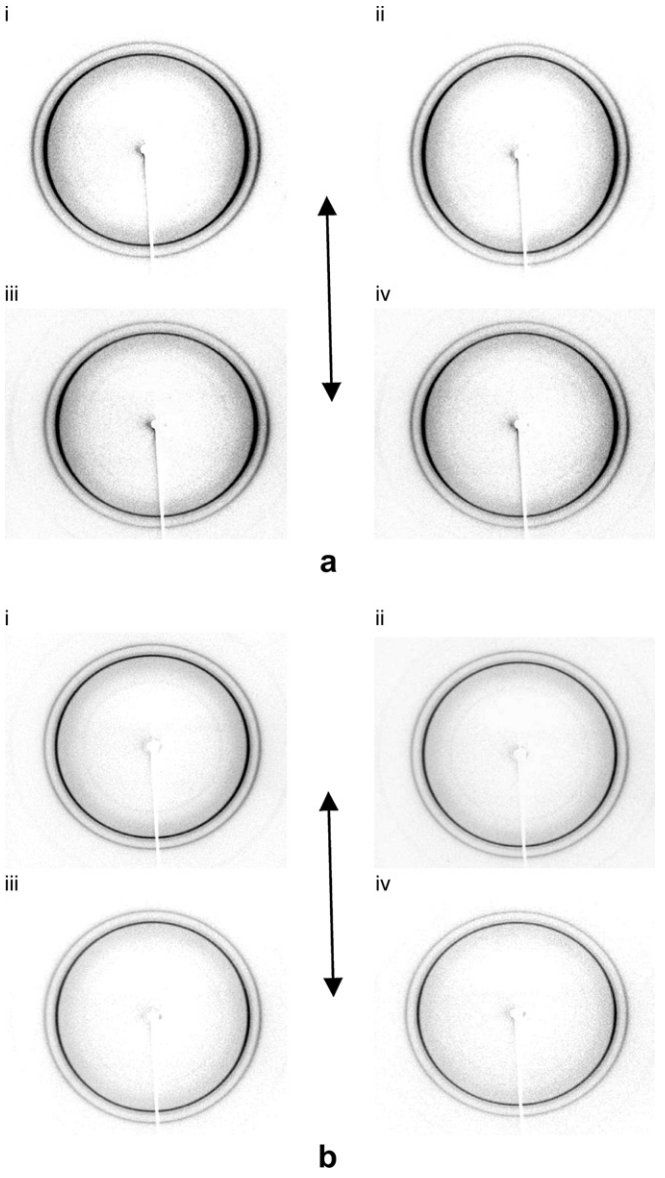

Fig. 12. WAXD pattern of (a) 250 nm aligned fibers at (i) 0 strain level%, (ii) 10 strain level%, (iii) 20 strain level%, (iv) 40 strain level% and (b) 900 nm aligned fibers at (i) 0 strain level% (ii) 10 strain level%, (iii) 20 strain level%, (iv) 40 strain level %. It can be seen from the figure that the fibers with 250 nm in diameter have better molecular orientation compared to fibers with 900 nm diameter. The arrow indicates the strain direction.

strained to 0, 10, 20 and 40%. The microstructural analyses at various elongation levels are performed to record any intrinsic structural changes at different strain levels (%). There are two strong diffraction arcs (or rings) at Bragg angles $2\theta = 21.6^\circ$ and 24° observed for all the samples tested. The equatorial peak at 21.6° is attributed to the diffraction of the (110) lattice plane and the peak at 24° is attributed to the (200) lattice plane, which is usually seen in orthorhombic semi-crystalline PCL [28]. The arc width of the strongest equatorial reflection provides an indication of the degree of orientation within the samples. It is clear from Fig. 12 that 900 nm-wide fibers have less degree of orientation compared to 250 nm-wide fibers, that is, the wider the fibers the less degree of molecular orientation is exhibited. It is clear that the electrospun fiber diameter has an influence on the molecular orientation and crystallinity. Fig. 13 illustrates the degree of crystallinity (%) vs. the fiber diameter at 0% straining. As can be seen, the change is gradual and continuous, and this is drastically different from those of Figs.

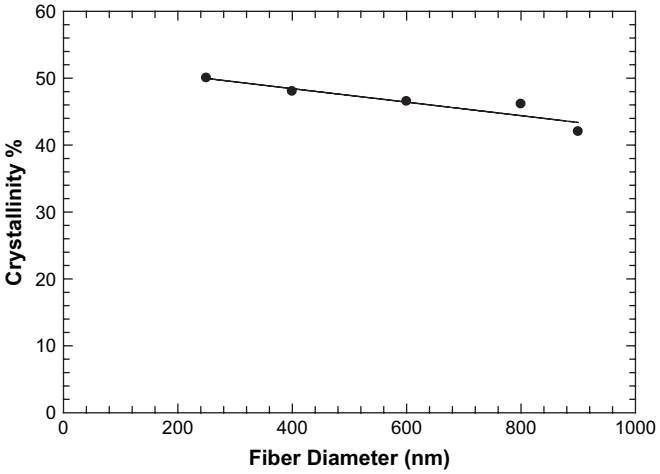

Fig. 13. Plots of crystallinity (%) vs. fiber diameter for aligned fibers at 0% strain. The degree of crystallinity increases gradually as the fiber diameter is reduced.

9–11, which strongly suggest the shifts in mechanical properties and thus the draw ratio is abrupt. Fig. 14 shows the degree of crystallinity (%) vs. straining level (%). The crystallinity increases with the reduction of fiber diameter and straining level (%). Fig. 15 indicates the degree of molecular orientation (%) vs. straining level (%). It can be verified from Fig. 15 that the molecules are better aligned along the axial direction upon straining. Molecular orientation determined from the WAXD study increases with a decrease in fiber diameter. We can readily confirm that electrospinning improves the degree of crystallinity and aligns the molecules in the direction of fiber axis. The polymer chains in the electrospun nanofibers undergo extensional deformation along the axial direction, which enhances molecular anisotropy [4,5,15] and result in the increase of the mechanical properties.

Despite these results corroborate the conjecture by Lim [24] and Chew [25] that molecular orientation enhances the crystal orientation of spun fibers, it cannot nonetheless ascertain why the gentle improvement in molecular orientation and crystallinity reported herein can give rise to an abrupt change in the draw ratio and tensile properties. It appears that crystalline morphology [7,25], which is not captured in the measurements of the molecular orientation and the degree of crystallinity reported herein could be crucial to the understanding of the transitional behavior around ~700 nm. The examination of crystalline morphology and supramolecular structures is beyond the scope of our discussion at present.

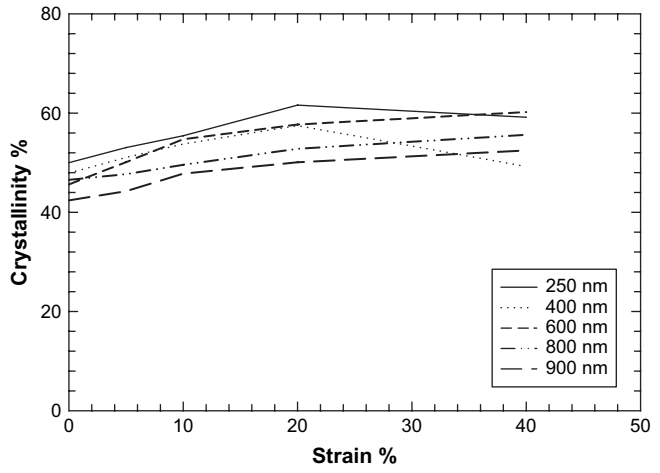

Fig. 14. Plots of crystallinity (%) vs. strain (%) obtained from WAXD analysis on aligned fibers. Fibers with smaller diameters show better crystallinity compared to larger diameter fibers.

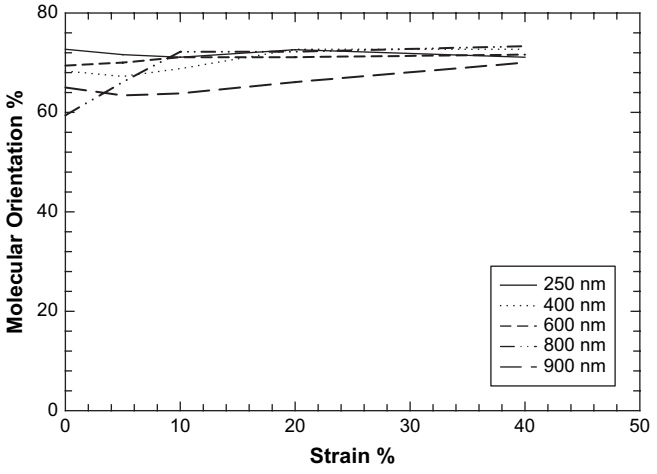

Fig. 15. Plots of molecular orientation (%) vs. strain (%) as obtained from WAXD analyses on aligned fibers. Fibers with smaller diameters are seen to have better molecular orientation compared to larger diameter fibers. It can be seen that the molecular orientation improves with strain (%).

3.5. Mechanical behavior of non-spun PCL–HAP composites

Fig. 16 shows the representative stress–strain curves of HAP filled PCL composites processed using extrusion followed by injection molding. All the specimens neck and elongate to

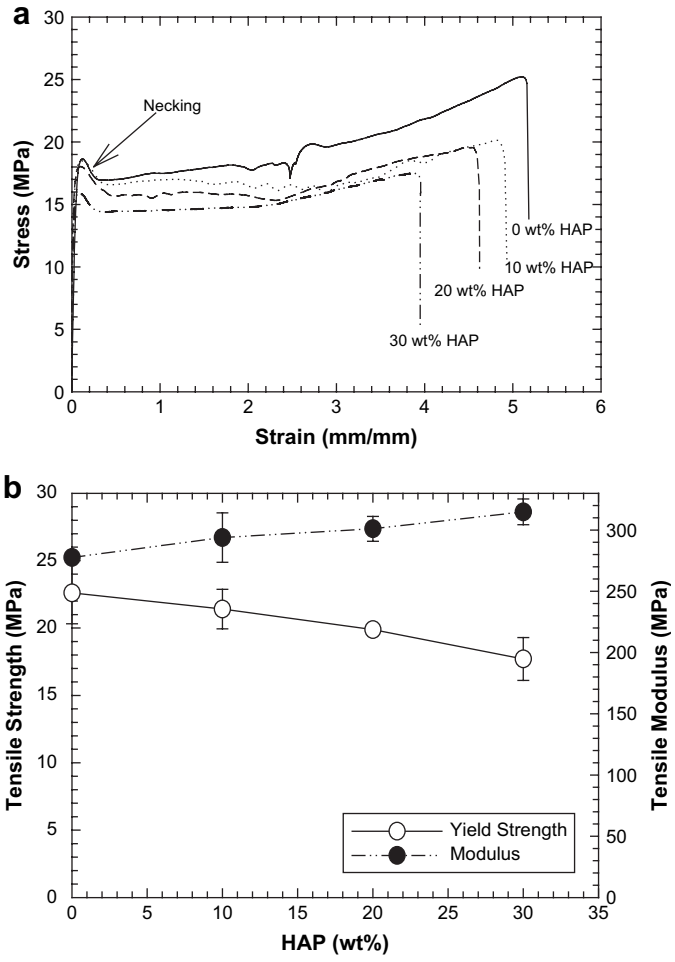

Fig. 16. (a) Representative stress–strain curves of HAP filled PCL composites. The samples are prepared using extrusion followed by compression molding process. (b) Plot of modulus and tensile strength vs. HAP wt% for non-spun samples.

a significant extent before failure (Fig. 16a). The tensile modulus for the specimens increases with increasing filler loading. However, the tensile strength decreases with filler loading as shown in Fig. 16b. This behavior is typical of many reinforced polymer specimens obtained using a top–down processing approach. The addition of HAP serves as weak links in PCL. These weak links become stress concentrators in a continuum matrix and thus reduce the tensile strength of the composites.

3.6. Mechanical behavior of spun PCL–HAP composites

Representative stress–strain curves of the spun HAP–PCL composites with increasing HAP concentration (0–30 wt%) are shown in Fig. 17a. Note that these sets of samples are inadvertently tested at a higher loading rate (10%/s) using MTS NanoBionix. The NanoBionix is specially designed for small load testing and it comes with a higher loading rate. Nevertheless the reinforcement trends are useful and they provide insights in understanding the distinct advantage in preparing nanofiber-architectural composite systems. The tensile modulus increases with increasing HAP concentration as shown in Fig. 17b. Interestingly, for these samples, the HAP addition increases the tensile strength. This is an important observation, differing from one expected from many discontinuous reinforcement systems. It, to a great extent, reflects the merits of a bottom–up approach for the electrospun polymer composites. In spun samples, the HAP particles are carried by the nanofibers and serve to constrain the segmental motion of the PCL chains, thus enhancing the tensile strength of the composites. This fiber-guided architecture creates a more effective reinforcement in comparison to filler-dispersion approach in Section 3.5. As evident from Fig. 17a, the stress–strain curves of these samples do not display necking phenomenon which is consistent with Fig. 4. This observation shows that the electrospinning process forces the molecular chains to reorder themselves in a fashion distinct from polymers processed in a melt flow fashion.

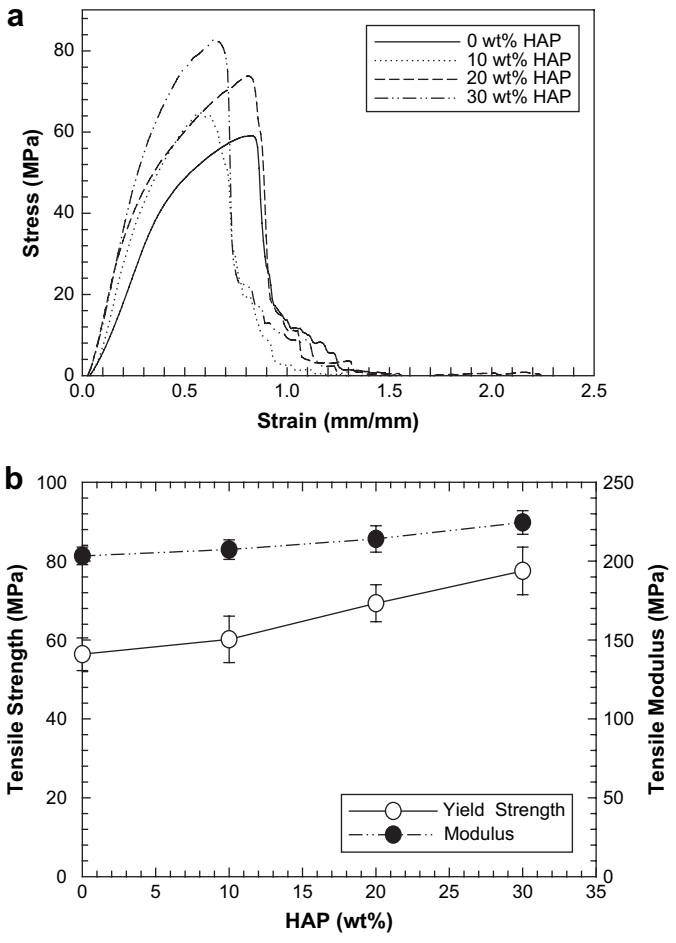

Fig. 17. (a) Representative stress–strain curves of spun PCL fibers with HAP inclusion (0–30 wt%). (b) Plot of modulus and tensile strength vs. HAP wt% for spun samples.

The modulus is assessed from the beginning of linear elastic deformation and is sensitive to the global deformation of the tested specimen. The high tensile strength values and unique stress–strain behavior displayed by the electrospun specimens can be attributed to enhanced anisotropy, molecular conformation and the transition from flaw-sensitive domain governed by Griffith's fracture mechanics [29] to less flaw-sensitive interfacial separation under theoretical strength as suggested by other investigators earlier [5,6].

4. Conclusions

The abrupt shift in tensile strength and stiffness of electrospun PCL fibers at around 700 nm reported in this paper illustrates the importance of studying the multiscale transition systematically by applying spatial confinement using the electrospinning techniques. Tensile strength, stiffness and draw ratio of electrospun PCL were increased, in an abrupt fashion, by decreasing the fiber diameter. From the WAXD study and draw ratio results, it is determined that reducing the fiber diameter improves the crystallinity and molecular orientation which explains the enhanced tensile properties for smaller diameter fibers. The abrupt shift in tensile properties was conjectured to arise from enhanced orderliness of the amorphous phase and crystalline morphology [24,25,27], or the presence of supramolecular structures [7], and the fiber diameter at which the abrupt shift in tensile properties occurs should be a characteristic of molecules examined. Future work will be focused on understanding the mechanical characteristics and thus modeling the tensile deformation of electrospun PCL nanofibers.

Acknowledgements

This work is supported by the National Science Foundation under the CAREER Award CMMI #0746703 and Award DMI # 0520967. The authors wish to thank Dr. T.A. Blackledge and Dr. D.H. Reneker for suggestions and useful discussions during the preparation of this paper. One of us (SCW) acknowledges the support from Dr. Andrew McGill during the tenure as a senior faculty fellow at the US. Naval Research Laboratory. The authors would like to thank the reviewers for constructive comments on improving this manuscript.

References

[1] Currey JD. The mechanical properties of biological materials. In: Currey JD, Vincent JFV, editors. S.E.B Symposium 34. Cambridge, UK; 1980. p. 75.
[2] Ji B, Gao H. Mater Sci Eng A 2004;366:93–103.
[3] Curry JD. Proc R Soc London Ser B 1977;196:443–63.
[4] Nalla RK, Krizic JJ, Kinney JH, Ritchie RO. Biomaterials 2005;26:217–31.
[5] Kendall K. Nature 1978;272:710–1.
[6] Ji B, Gao H, Buehler MJ, Yao H. Mech Chem Biosys 2004;1:37–52.
[7] Arinstein A, Burman M, Gendelman O, Zussman E. Nat Nanotech 2007;2:59–62.
[8] Katti KS, Katti DS. Mater Sci Eng Part C Bio S 2006;26:1317–24.
[9] Evans AG, Suo Z, Wang RZ, Aksay IA, He YW, Hutchinson JW. J Mater Res 2001;16:2475–84.
[10] Baji A, Wong SC, Blackledge TA, Leng S. Proceedings of annual technical conference – Society of Plastics Engineers, ANTEC, 2008. Milwaukee, Wisconsin USA; May 4–8 2008.
[11] Wong SC, Baji A, Tripatanasuwan S, Blackledge T, Reneker D. ASME international mechanical engineering congress and exposition. Seattle, Washington USA; Nov 2007.
[12] Wu J, Mai YW. Polym Eng Sci 1996;18:2275–88.

[13] Mai YW, Wong SC, Chen XH. In: Paul DR, Bucknall CB, editors. Application of fracture mechanics for characterization of toughness of polymer blends, vol. 2. New York: Wiley; 2000. p. 17–58 [chapter 20].
[14] Zussman E, Burman M, Yarin AL, Khalfin R, Cohen Y. J Polym Sci Part B Polym Phys 2006;44:1482–9.
[15] Reneker DH, Chun I. Nanotechnology 1996;7:216–23.
[16] Doshi J, Reneker DH. J Electrostat 1995;35:151–60.
[17] Pham PQ, Sharma U, Mikos AG. Biomacromolecules 2006;7:2796–805.
[18] White JL, Hancock TA. J Appl Polym Sci 1981;21:3157–70.
[19] Brazinsky I, Williams AG, LaNieve HL. Polym Eng Sci 1975;15:834–41.
[20] Wang H, Shao H, Hu X. J Appl Polym Sci 2006;101:961–8.
[21] Fennessey SF, Farris RJ. Polymer 2004;45:4217–25.
[22] Ngai KL. J Polym Sci Part B Polym Phys 2006;44:2980–95.
[23] Ngai KL. Eur Phys J E 2002;8:225–35.
[24] Lim CT, Tan EPS, Ng SY. Appl Phys Lett 2008;92:1–3.
[25] Chew SY, Hufnagel TC, Lim CT, Leong KW. Nanotechnology 2006;17: 3880–91.
[26] Jin KS, Heo K, Oh W, Yoon J, Lee B, Hwang Y, et al. J Appl Crystallogr 2007; 40:s631–6.
[27] Qiao C, Jiang S, Ji X, An L, Jiang B. Front Chem Chin 2007;2:343–8.
[28] Bittiger H, Marchessault RH, Niegisch WD. Acta Crystallogr B 1970;26:1923–7.
[29] Griffith AA. Philos Trans R Soc London Ser A 1920;221:163–98.